NANO LETTERS

pubs.acs.org/NanoLett Letter

$RuCoO_x$ Nanofoam as a High-Performance Trifunctional Electrocatalyst for Rechargeable Zinc–Air Batteries and Water Splitting

Chenhui Zhou, Siming Zhao, Haibing Meng, Ying Han, Qinyuan Jiang, Baoshun Wang, Xiaofei Shi, Wenshuo Zhang, Liang Zhang, and Rufan Zhang*

Cite This: *Nano Lett.* 2021, 21, 9633–9641 Read Online

ACCESS | Metrics & More | Article Recommendations | Supporting Information

ABSTRACT: Designing high-performance trifunctional electrocatalysts for ORR/OER/HER with outstanding activity and stability for each reaction is quite significant yet challenging for renewable energy technologies. Herein, a highly efficient and durable trifunctional electrocatalyst $RuCoO_x$ is prepared by a unique one-pot glucose-blowing approach. Remarkably, $RuCoO_x$ catalyst exhibits a small potential difference (ΔE) of 0.65 V and low HER overpotential of 37 mV (10 mA cm^{-2}), as well as a negligible decay of overpotential after 200 000/10 000/10 000 CV cycles for ORR/OER/HER, all of which show overwhelming superiorities among the advanced trifunctional electrocatalysts. When used in liquid rechargeable Zn–air batteries and water splitting electrolyzer, $RuCoO_x$ exhibits high efficiency and outstanding durability even at quite large current density. Such excellent performance can be attributed to the rational combination of targeted ORR/OER/HER active sites into one electrocatalyst based on the double-phase coupling strategy, which induces sufficient electronic structure modulation and synergistic effect for enhanced trifunctional properties.

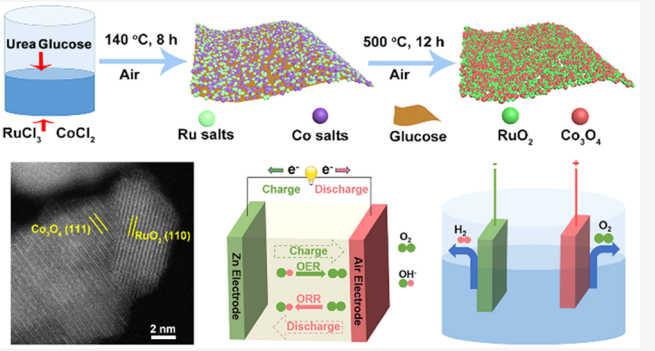

KEYWORDS: *multifunctional electrocatalysts, porous nanofoam-like oxide, double-phase coupling effects, Zn–air batteries, water splitting*

Downloaded via TSINGHUA UNIV on November 30, 2021 at 12:54:30 (UTC).
See https://pubs.acs.org/sharingguidelines for options on how to legitimately share published articles.

The ever-growing global energy and environmental problems motivate people to develop clean and sustainable energy devices including water splitting, rechargeable metal–air batteries, and fuel cells for reducing CO_2 emission.[1−7] The hydrogen evolution reaction (HER) and oxygen evolution reaction (OER) are the two critical electrochemical reactions for water splitting, while the oxygen reduction reaction (ORR) and OER are recognized as the two key electrochemical processes for rechargeable metal–air batteries.[8−10] However, these three reactions are sluggish in kinetics and always need large overpotential since multielectron transfer is always involved, which urge the development of high-efficient electrocatalysts to accelerate the reactions. Many efforts have been devoted to explore electrocatalysts with single functionality, such as Pt/Pd-based alloys and M–N–C single-atom catalysts for ORR,[11,12] Ir/Ru-based materials and NiFe-LDH for OER,[13,14] and Pt-based materials and MoS_2 for HER.[15,16] Currently, developing electrocatalysts with multifunctionality while maintaining high catalytic performance for each reaction is an urgent yet challenging task,[17,18] since using different catalysts for cathodic and anodic reactions usually cause many problems, which complicate the device construction, sacrifice the whole properties, and increase the costs.[19] For instance, bifunctional ORR/OER catalysts are needed in the cathode of the rechargeable metal–air batteries, since ORR and OER reactions occur alternately in the cathode during the discharging and charging process. If two different electrocatalysts such as the compounds of Pt/C and RuO_2/IrO_2 are loaded on the cathode, the active sites for each reaction would be diluted. Additionally, the ORR/OER components may be oxidized/reduced in the constantly switched OER (charging) and ORR (discharging) processes, resulting in the deterioration of catalyst performance.[20] For water splitting systems, the exploitation of bifunctional HER/OER catalysts is highly desired, since the device can be simplified for reducing cost.[21] Therefore, the design of multifunctional electrocatalysts with high ORR/OER/HER performance shows great significance when applied in rechargeable metal–air batteries and water splitting.

Received: September 2, 2021
Revised: November 5, 2021
Published: November 11, 2021

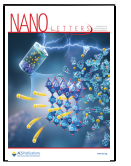

ACS Publications © 2021 American Chemical Society

https://doi.org/10.1021/acs.nanolett.1c03407
Nano Lett. 2021, 21, 9633–9641

Scheme 1. Illustration of the Preparation of Foam-like $RuCoO_x$

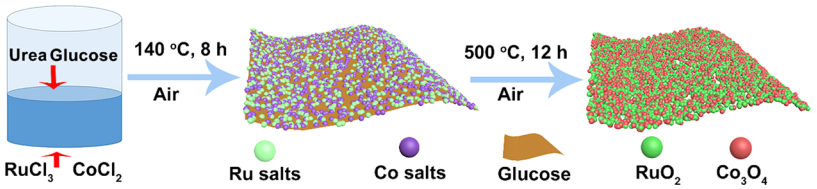

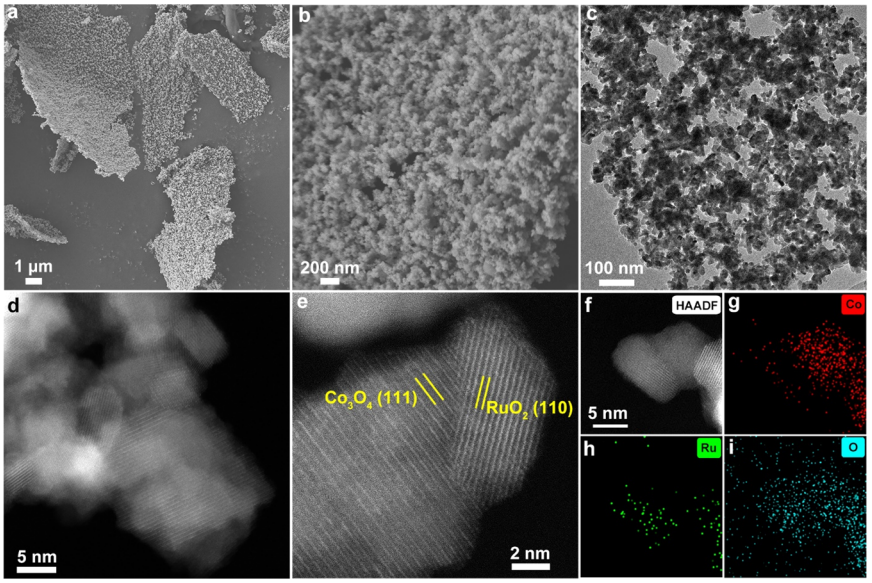

Figure 1. Morphology, structure, and composition characterization of $RuCoO_x$ catalyst: (a, b) SEM and (c) TEM images showing the foam-like structures of $RuCoO_x$; (d) HAADF-STEM image showing the structure of foam-like $RuCoO_x$ consisting of small crystals; (e) HAADF-STEM of $RuCoO_x$ showing the interfacial structure between the adjacent RuO_2 and Co_3O_4 crystals; (f–i) elemental mapping images of $RuCoO_x$ showing the inhomogeneous distribution of Co and Ru.

Recently, several multifunctional electrocatalysts have been reported, including non-noble or noble metal catalysts. Non-noble metal catalysts usually involve iron, cobalt, and nickel-based alloys/oxides/phosphides/sulfides/carbides/nitrides coupled with carbon substrate, such as CoFe@NC/NCHNSs,[22] Ni-NiO/N-rGO,[23] FeCo/Co_2P@NPCF,[24] Co_2P/CoNPC,[25] FeS/Fe_3C@N-S-C,[26] Fe_2N/S/N,[27] etc. However, these non-noble metal catalysts still exhibit insufficient activities and durability, especially when used as trifunctional electrocatalysts for ORR/OER/HER simultaneously. It is quite challenging to achieve the target of half-wave potential ($E_{1/2}$) larger than 0.85 V for ORR, the overpotential at 10 mA cm^{-2} smaller than 300/50 mV for OER/HER at the same time.[28] Some researchers focus on the design of noble metal trifunctional electrocatalysts, including PtCo/Ir,[29] Rh_6Cu,[30] etc. Although these catalysts can partially achieve some of the above targets, the high cost of these Pt/Ir/Rh-based materials significantly limits their wide applications. Among the noble metals, Ru is much cheaper than Pt/Pd/Ir/Rh. Some Ru-based systems containing RuP/NPC,[31] 0.4-Ru@NG-750,[32] and Ru@NGA-900[33] have also been explored as ORR/OER/HER trifunctional electrocatalysts, while these materials can still hardly meet the harsh requirements. The challenge for the development of Ru-based trifunctional catalysts mainly exists in the ORR performance, since pure Ru-based materials exhibit unsatisfactory ORR performance due to the improper electronic structure.[34] Additionally, achieving enhanced OER/HER activities through regulating the ORR performance is also a challenging task.

Herein, a unique double-phase coupling strategy is proposed to construct $RuCoO_x$ bimetallic oxides, which show superiorities in the aspects of rational screening of targeted ORR/OER/HER sites, sufficient electronic structure modulation and synergistic function induced by double-phase coupling effects, and long-term material and structural stability. The rationally designed $RuCoO_x$ catalyst shows excellent trifunctional catalytic activities and stability for ORR, OER, and HER simultaneously, with a small ΔE of only 0.65 V and an overpotential of 37 mV to reach 10 mA cm^{-2} for HER. The catalysts were further extended for practical applications including rechargeable zinc–air batteries and water splitting, which also exhibit high efficiency and excellent durability even at quite large current density. This work paves a feasible way to rationally integrating various active sites to construct multifunctional electrocatalysts for rechargeable metal–air batteries and water splitting.

The synthesis process of the $RuCoO_x$ nanofoam is schematically illustrated in Scheme 1. Glucose, urea, ruthenium chloride, and cobalt chloride were first dissolved in DI water to form a uniform solution, which was subsequently settled at 140 °C for 8 h. During the heating process, glucose gradually turned into molten syrup with homogeneous distribution of the metal salts and formed a porous foam consisting of bubble walls due to the gas releasing from the decomposition of urea. The glucose template was then removed by calcination at 500 °C for 12 h in air to form the $RuCoO_x$ nanofoam.

The morphology of $RuCoO_x$ was characterized by field-emission scanning electron microscopy (SEM) and trans-

https://doi.org/10.1021/acs.nanolett.1c03407
Nano Lett. 2021, 21, 9633–9641

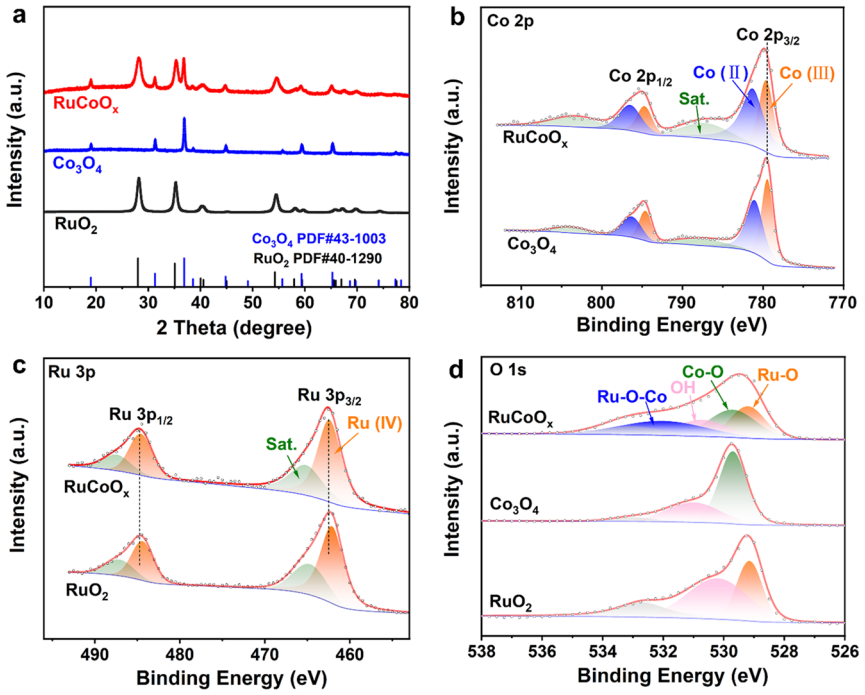

Figure 2. XRD and XPS characterization of $RuCoO_x$, RuO_2, and Co_3O_4: (a) XRD patterns indicating the phase constitution of $RuCoO_x$ by RuO_2 and Co_3O_4; XPS spectra of (b) Co 2p for $RuCoO_x$ and Co_3O_4, (c) Ru 3p for $RuCoO_x$ and RuO_2, and (d) O 1s for $RuCoO_x$, Co_3O_4, and RuO_2.

mission electron microscopy (TEM). As shown in Figures 1a and S1a, the as-prepared $RuCoO_x$ exhibits sheet-like structures at low magnification, and a unique porous foam-like structure can be further observed at high magnification (Figure 1b,c, Figure S1b), which benefits the improvement of catalytic performance. The specific surface area (S_{BET}) of the $RuCoO_x$ nanofoam was determined to be 31.81 $m^2\ g^{-1}$ by Brunauer–Emmett–Teller (BET) tests (Figure S2). For comparison, pure RuO_2 and Co_3O_4 with similar porous foam-like structure were also prepared using a similar procedure except for changing the metal salts to $RuCl_3$ and $CoCl_2$, respectively (Figures S3 and S4). High-angle annular dark-field scanning transmission electron microscopy (HAADF-STEM) images displayed that the synthesized $RuCoO_x$ nanofoam was constituted of small crystals (Figure 1d, Figure S5), and the adjacent two crystals represent different phase structures, which can be ascribed to the (110) plane of RuO_2 and (111) plane of Co_3O_4 (Figure 1e, Figure S6). Additionally, the RuO_2 nanocrystal is closely coupled with Co_3O_4 nanocrystals, which induce electronic structure modulation and synergistic effects for enhanced catalytic performance. Energy dispersive spectra (EDS) mapping images reveal that the O element exhibits homogeneous distribution, while Ru/Co elements show distinct distribution with few Co atoms dispersed into RuO_2 crystal (Figure 1f,i, Figure S7), which further verifies the coupling effects between RuO_2 and Co_3O_4 nanocrystals.

X-ray diffraction (XRD) shows the coexistence of RuO_2 (PDF no. 40-1290) and Co_3O_4 (PDF no. 43-1003) for the $RuCoO_x$ nanofoam (Figure 2a), and the prepared pure RuO_2 and Co_3O_4 catalysts correspond to RuO_2 (PDF no. 40-1290) and Co_3O_4 (PDF no. 43-1003), respectively. X-ray photoelectron spectroscopy (XPS) was carried out to reveal the valence states of the electrocatalysts. The high-resolution Co 2p XPS spectrum of the $RuCoO_x$ nanofoam can be deconvoluted into signals at 779.65 and 794.55 eV ascribed to the Co^{3+} $2p_{3/2}$ and $2p_{1/2}$ and signals at 781.35 and 796.6 eV corresponding to the Co^{2+} $2p_{3/2}$ and $2p_{1/2}$, respectively (Figure 2b).[35] The peaks of Co 2p in $RuCoO_x$ show a positive shift, and the peak area of Co^{2+} increased compared with the pure Co_3O_4, indicating the strong electronic interaction between RuO_2 and Co_3O_4. Figure 2c shows that the peaks of Ru 3p in $RuCoO_x$ exhibit a positive shift compared with the pure RuO_2, which implies that the Co_3O_4 can obtain the electrons from RuO_2. The high-resolution O 1s spectrum of the $RuCoO_x$ nanofoam can be deconvoluted into signals at 529.2, 529.75, and 532.1 eV, which correspond to the Ru–O, Co–O, and Ru–O–Co bonds (Figure 2d), respectively.[36] The formation of the Ru–O–Co bond could be ascribed to the strong interaction between RuO_2 and Co_3O_4, which serves as the channel of electron transfer from Ru to Co and has benefits for the electronic structure adjustment.

The oxygen reduction reaction (ORR) performance was first assessed by linear sweep voltammetry (LSV). $RuCoO_x$ nanofoam shows excellent ORR activity with a large $E_{1/2}$ of 0.855 V (Figure 3a), which is comparable to commercial Pt/C catalysts of 0.85 V, and shows superiority toward those of pure RuO_2 and Co_3O_4, as well as the recently reported Co_3O_4-based electrocatalysts (Table S1). Meanwhile, the Tafel slope of $RuCoO_x$ nanofoam (46.7 mV dec^{-1}) is also much smaller than commercial Pt/C, pure RuO_2 and Co_3O_4 catalysts (inset of Figure 3a), indicating the enhanced ORR reaction kinetics. The reaction is close to a four-electron transfer process since the electron transfer number is approaching 4 and H_2O_2 yield is lower than 2% (Figure S8). Furthermore, accelerated stability tests (ADT) was conducted to assess the stability of the catalyst. Remarkably, the $RuCoO_x$ nanofoam exhibits excellent long-term durability with a negligible degradation of $E_{1/2}/J_L$ (limited current density) even after 200 000 CV cycles (Figure 3b,c), and a small decay of current density after 10 h chronoamperometry tests (Figure S9). This cycling number of 200 000 shows overwhelming superiority to the previously reported cycling numbers (Tables S1 and S2). Such out-

https://doi.org/10.1021/acs.nanolett.1c03407
Nano Lett. 2021, 21, 9633–9641

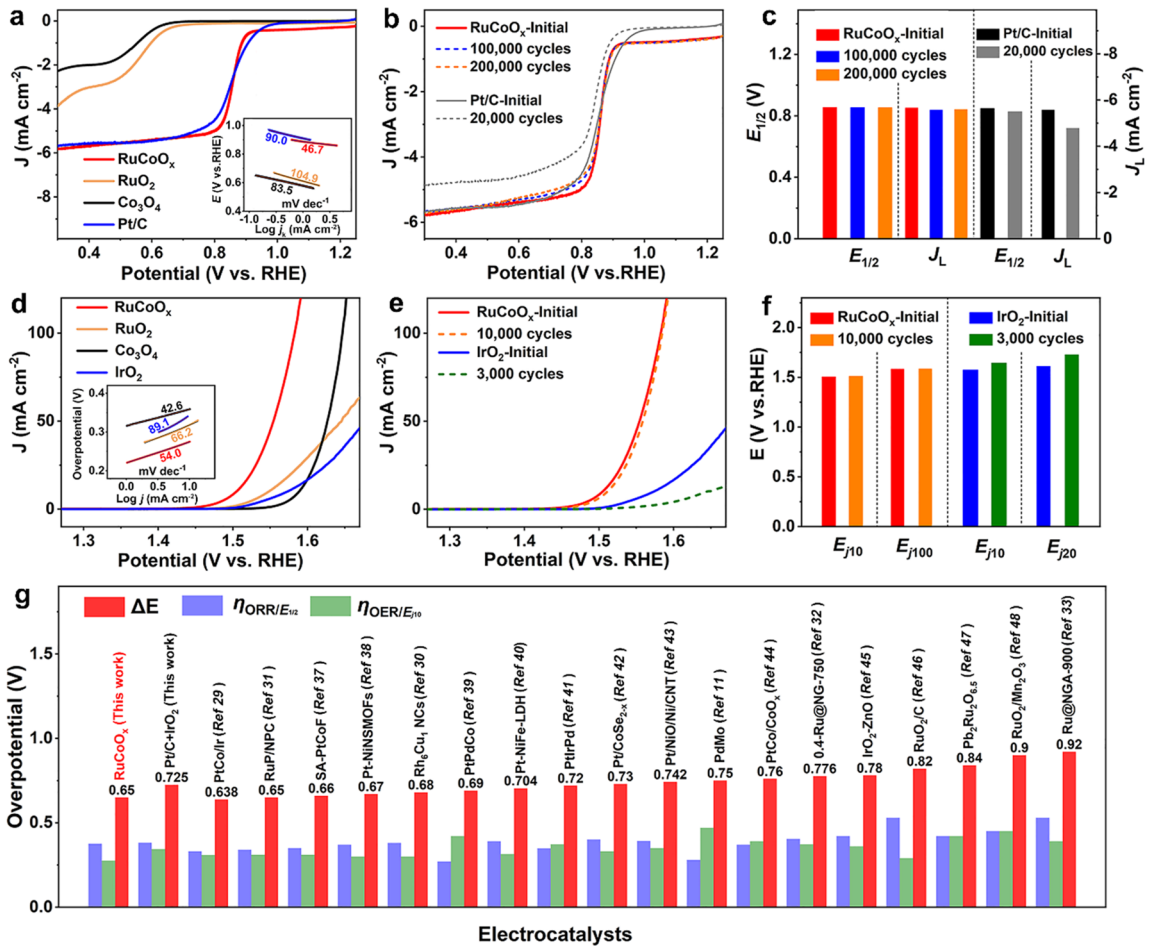

Figure 3. Electrocatalytic performance of $RuCoO_x$ for ORR and OER: (a) LSV curves and corresponding Tafel plots (inset) of ORR for $RuCoO_x$, RuO_2, Co_3O_4, and Pt/C obtained at 1600 rpm; (b) LSV curves of $RuCoO_x$ and Pt/C before and after various potential cycles; (c) $E_{1/2}$ and J_L before and after various potential cycles for $RuCoO_x$ and Pt/C; (d) OER LSV curves and Tafel plots of $RuCoO_x$, RuO_2, Co_3O_4, and IrO_2 obtained at 1600 rpm; (e) LSV curves of $RuCoO_x$ and IrO_2 before and after various potential cycles; (f) OER potential of E_{j10}/E_{j100} for $RuCoO_x$ and E_{j10}/E_{j20} for IrO_2 before and after various potential cycles; (g) comparison of the overpotential for ORR, OER, and ΔE ($\Delta E = E_{j10} - E_{1/2}$) between $RuCoO_x$ and other catalysts.

standing stability of $RuCoO_x$ can be explained by the maintained structure after CV tests (Figure S10).

The $RuCoO_x$ nanofoam also displayed high OER activities with an overpotential of 275 mV (10 mA cm^{-2}) as shown in Figure 3d, surpassing that of commercial IrO_2 catalysts, pure RuO_2 and Co_3O_4 catalysts. Moreover, the $RuCoO_x$ nanofoam possessed fast OER kinetics with a low Tafel slope of 54 mV dec^{-1} (inset in Figure 3d). The $RuCoO_x$ catalyst also exhibited superior OER stability than IrO_2 with a small shift of only 6 mV at 10 mA cm^{-2} after 10 000 cycling tests and an increase in overpotential of just 43 mV after chronopotentiometry tests for 10 h (Figure 3e,f, Figure S11). The maintained structure after CV tests confirms the excellent durability of $RuCoO_x$ for OER (Figure S12). The potential difference (ΔE) ($\Delta E = E_{j10} - E_{1/2}$) of the OER and ORR was a general index to evaluate the bifunctionality of oxygen electrode catalysts. The $RuCoO_x$ electrocatalyst showed a small ΔE of 0.65 V (Figure S13), which was smaller than those of commercial Pt/C + IrO_2, pure RuO_2 and Co_3O_4 electrocatalysts, and outperformed nearly all of the advanced bifunctional oxygen catalysts[11,29−33,37−48] (Figure 3g, Table S2).

The origin of the excellent ORR and OER performance were further discussed as below. The ORR performance of $RuCoO_x$ electrocatalyst may be mainly contributed by Co_3O_4, since the pure RuO_2 exhibited low ORR activity.[49] Co_3O_4 has been investigated as an ORR electrocatalyst for a long time,[50,51] while the $E_{1/2}$ can hardly reach 0.85 V due to the weak adsorption of Co sites toward oxygenated intermediates. It has been proven by XPS that the peaks of Co 2p in $RuCoO_x$ showed a positive shift toward the pure Co_3O_4, indicating the increased concentration of low-stated Co for a reduced valence state. Recent research studies showed that low-valence metal cations in the metal oxides possessed higher surface reactivity due to the unpaired d-electrons, which enhanced the oxygen adsorption due to the increased energy of E_d (coupling of O 2p to the highest occupied d-states).[34,49] Therefore, the $RuCoO_x$ catalyst exhibited enhanced ORR performance compared with the pure Co_3O_4. The OER performance of the $RuCoO_x$ electrocatalyst can be contributed by RuO_2 and Co_3O_4 simultaneously. These two components both exhibit excellent OER performance, and the pure RuO_2 exhibits a smaller onset potential than Co_3O_4, while the Co_3O_4 shows a faster OER reaction kinetics than the RuO_2 due to the lower Tafel slope. Therefore, the $RuCoO_x$ electrocatalyst can integrate the advantages of both smaller onset potential of RuO_2 and fast

https://doi.org/10.1021/acs.nanolett.1c03407
Nano Lett. 2021, 21, 9633−9641

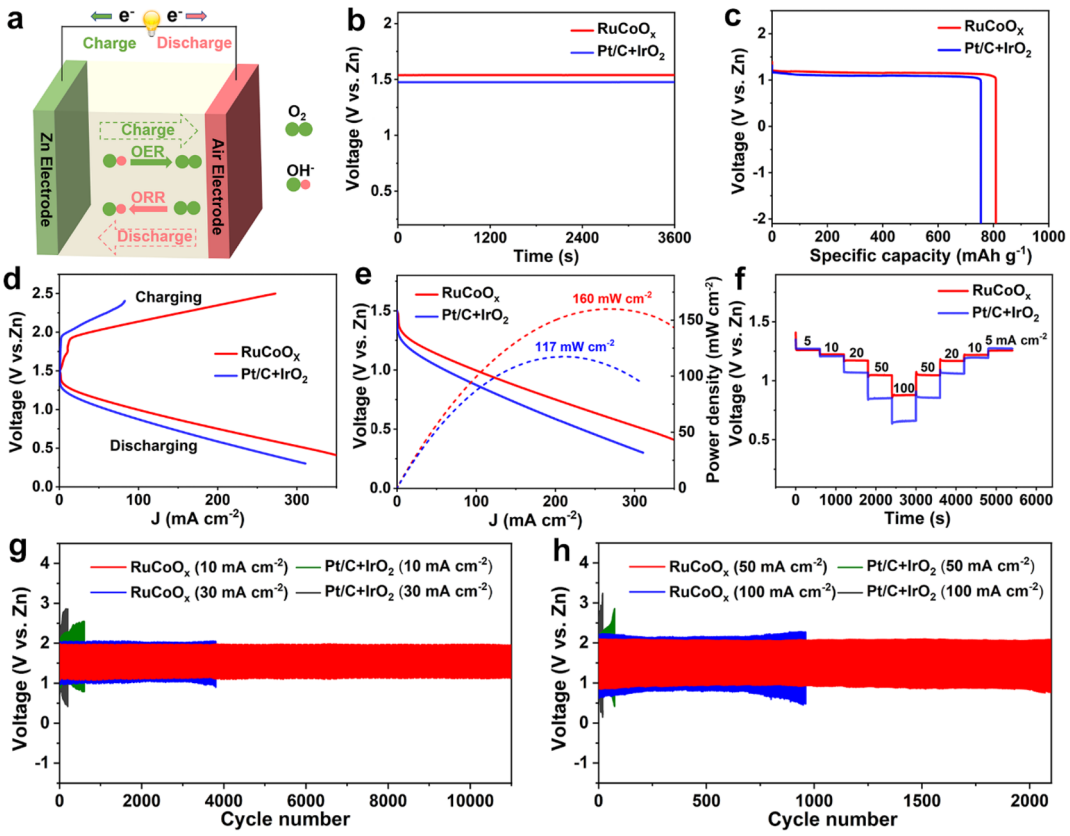

Figure 4. Performances of Zn−air batteries using different cathodic catalysts: (a) scheme of an aqueous Zn−air battery (ZAB); (b) open-circuit plots and (c) Zn mass-normalized specific capacities of Zn−air batteries using $RuCoO_x$ and Pt/C + IrO_2 as the cathodic catalysts; (d) charging and discharging curves; (e) power density curves and (f) discharging curves at various current densities of the Zn−air batteries using $RuCoO_x$ and Pt/C + IrO_2 as the cathodic catalysts; galvanostatic cycling tests of the Zn−air batteries operating at current densities of (g) 10 and 30 mA cm^{-2} and (h) 50 and 100 mA cm^{-2}.

OER reaction kinetics of Co_3O_4, giving rise to boosted OER performance.

The superior bifunctional activities and durability of the $RuCoO_x$ electrocatalyst motivated us to investigate its practical properties in rechargeable Zn−air batteries (Figure 4a, Figure S14). The $RuCoO_x$-based battery showed a large open-circuit voltage of 1.54 V (Figure 4b), a high specific capacity of 811.2 mAh g_{Zn}^{-1} (Figure 4c), which exceeded the Pt/C + IrO_2 based batteries (1.47 V, 754.7 mAh g_{Zn}^{-1}). The $RuCoO_x$-based battery exhibited a smaller discharge−charge overpotential than that of the Pt/C + IrO_2 cathode at various current densities (Figure 4d). Besides, the $RuCoO_x$-based battery also possessed a higher peak power density of 160 mW cm^{-2}, clearly outperforming the Pt/C + IrO_2 cathode of 117 mW cm^{-2} (Figure 4e). Figure 4f shows that the rate performance of $RuCoO_x$-based battery is superior to that of Pt/C + IrO_2 based battery with higher discharging voltages especially at large current densities. The long-term durability of the $RuCoO_x$-based battery was assessed by continuous galvanostatic discharging/charging cycling tests with 5 min discharging and 5 min charging. The long-term durability tests showed that the $RuCoO_x$-based battery could afford an ultralong lifespan of 11 000 cycles (corresponding to 1833.3 h) at 10 mA cm^{-2} without any obvious increase of voltage gaps (Figure 4g), while the Pt/C + IrO_2 based battery showed a significant increase of voltage gaps after only 600 cycles (100 h). Such outstanding stability exceeds nearly all of the reported cathode electrocatalysts (Table S2), suggesting that $RuCoO_x$ is highly promising to accomplish high-performance rechargeable Zn−air batteries. Impressively, when the cycling current densities were further increased to 30, 50, and 100 mA cm^{-2}, the $RuCoO_x$-based batteries could still operate for 3800 cycles (633.3 h), 2100 cycles (350 h), and 960 cycles (160 h), respectively, without obvious decay in performance (Figure 4g,h). As far as we know, operating at an ultrahigh current density of 100 mA cm^{-2} for a long time has never been reported for Zn−air batteries, and even cycling at 30 and 50 mA cm^{-2} was also rarely reported (Table S2), further demonstrating its outstanding durability in large current density application.

Finally, the $RuCoO_x$ electrocatalyst also exhibits excellent HER performance with an overpotential of only 37 and 112 mV to achieve 10 and 100 mA cm^{-2}, which is comparable to the commercial Pt/C catalyst of 23 and 141 mV and better than pure RuO_2 and Co_3O_4 catalysts (Figure 5a). The corresponding small Tafel slope (53.2 mV dec^{-1}) also indicates the fast HER reaction kinetics for $RuCoO_x$ (inset in Figure 5a). The long-term ADT and chronopotentiometry tests confirm the excellent HER stability of the $RuCoO_x$ catalyst with a negligible overpotential shift of only 1 mV at 10 mA cm^{-2} after 10 000 cycling tests and just 11 mV overpotential increase after chronopotentiometry tests for 10 h (Figure 5b,c, Figure S15). Since the metallic oxides exhibit phase transition under the negative potential, the actual active sites for HER were further explored. Recent studies indicate that the surface of RuO_2 can be reduced to metallic Ru under the HER potential, which

https://doi.org/10.1021/acs.nanolett.1c03407
Nano Lett. 2021, 21, 9633−9641

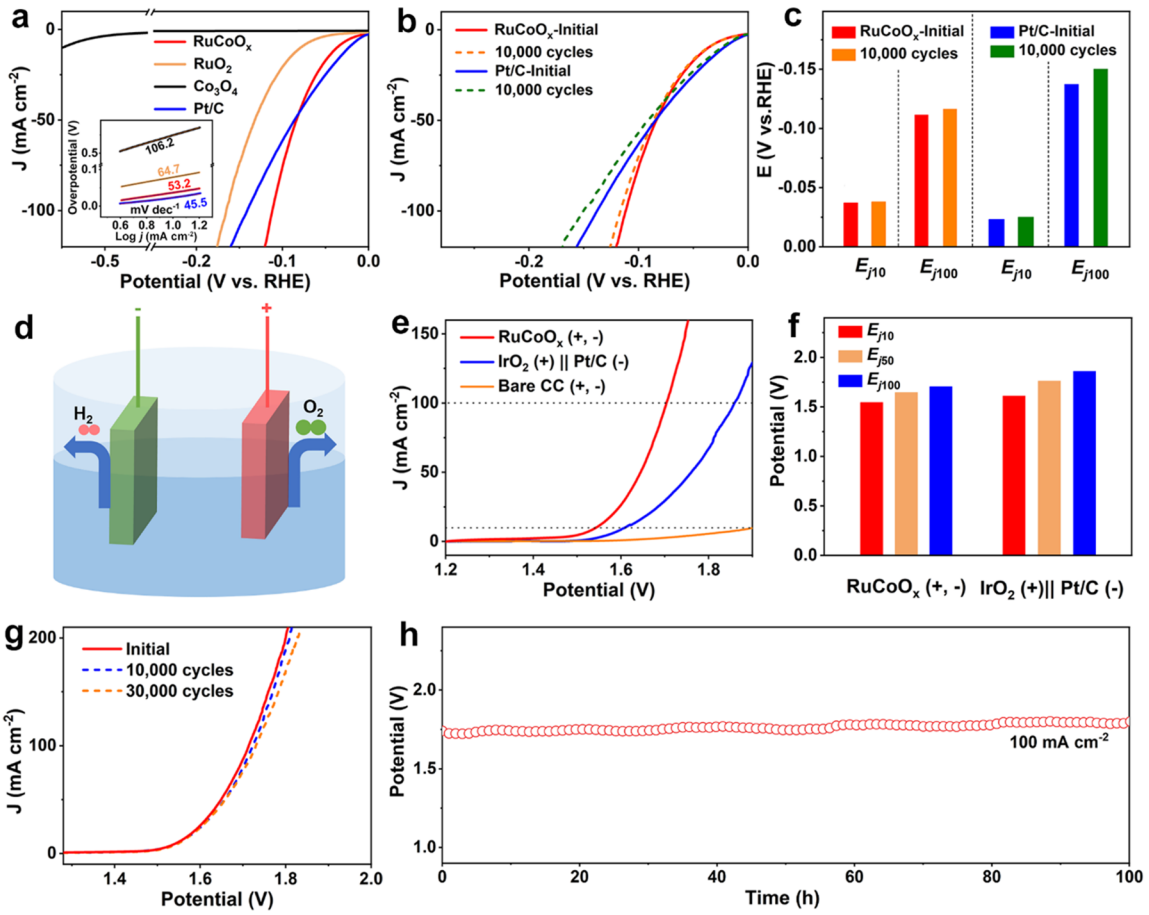

Figure 5. HER and overall water splitting performances: (a) LSV curves and corresponding Tafel plots of HER for $RuCoO_x$, RuO_2, Co_3O_4, and Pt/C obtained at 1600 rpm; (b) LSV curves of $RuCoO_x$ and Pt/C before and after various potential cycles; (c) HER potential of E_{j10} and E_{j100} for $RuCoO_x$ and Pt/C before and after various potential cycles; (d) scheme of the overall water splitting systems; (e) polarization curves and (f) comparison of the $E_{j10}/E_{j50}/E_{j100}$ between $RuCoO_x$ (+, −) and IrO_2 (+)||Pt/C (−); (g) polarization curves of $RuCoO_x$ for overall water splitting after 30 000 cycles; (h) chronopotentiometry test of $RuCoO_x$ for the water splitting device.

serves as the active sites for the HER,[52] while for the $RuCoO_x$ catalyst, $Co(OH)_2$ was detected after HER tests (Figures S16 and S17),[53] which can accelerate the kinetics of water dissociation for enhanced HER performance.[54]

Considering the excellent HER and OER performance of $RuCoO_x$, we assembled a two-electrode electrolyzer using $RuCoO_x$ as both anode and cathode for actual application (Figure 5d). The $RuCoO_x$ electrode needed a low potential of only 1.54 V to drive 10 mA cm^{-2}, which was lower than the electrode using commercial Pt/C and IrO_2 (Figure 5e,f). The $RuCoO_x$ electrode also showed excellent stability as evidenced by negligible potential shift of only 5 mV at 10 mA cm^{-2} after 30 000 cycling tests (Figure 5g). In addition, the $RuCoO_x$ electrode also maintained a constant potential when operating at 100 mA cm^{-2} for 100 h (Figure 5h). Such performances surpass most of the HER/OER bifunctional electrocatalysts (Table S3), indicating its promising application in water splitting.

In addition, as a trifunctional electrocatalyst, $RuCoO_x$ also shows superiority among the reported catalysts with low overpotential for ORR, OER, and HER (Table S4), which can achieve the harsh target of $E_{1/2}$ larger than 0.85 V for ORR, the overpotential at 10 mA cm^{-2} smaller than 300/50 mV for OER/HER at the same time. Combined with the outstanding behavior in long-term stability, highly efficient and durable devices including zinc−air batteries and water splitting electrolyzer were constructed, which show superiority especially at ultrahigh current density. Such excellent performance can be explained by the rational material and structural design based on the unique double-phase coupling strategy, which not only induces sufficient electronic structure modulation for enhanced catalytic activity but also endows the $RuCoO_x$ catalyst with excellent material and structural stability.

In summary, a facile one-pot glucose-blowing approach was developed to synthesize a $RuCoO_x$ nanofoam, which exhibited significantly enhanced trifunctional performances. The ΔE was only 0.65 V and the overpotential for HER was 37 mV (10 mA cm^{-2}), which exceeded most of the state-of-the-art trifunctional catalysts. The corresponding Zn−air batteries exhibited a large power density of 160 mW cm^{-2} and could cycle for 11 000/3800/2100/960 cycles at 10/30/50/100 mA cm^{-2}. The water splitting electrolyzer only needs 1.54 V to drive 10 mA cm^{-2} and could work at 100 mA cm^{-2} for 100 h without obvious increase of overpotential. Such excellent performance can be explained by the rational integration of ORR/OER/HER active sites into the $RuCoO_x$ catalyst and optimization of electronic structure by utilization of the coupling effect with synergistic function between the RuO_2 and Co_3O_4 nanocrystals. This work opens a new way toward the design of advanced trifunctional electrocatalyst with superior performance for the application in clean and sustainable energy technologies.

https://doi.org/10.1021/acs.nanolett.1c03407
Nano Lett. 2021, 21, 9633−9641

■ ASSOCIATED CONTENT

Supporting Information

The Supporting Information is available free of charge at https://pubs.acs.org/doi/10.1021/acs.nanolett.1c03407.

Experimental details; additional SEM, BET, HAADF-STEM, EDS mapping data; H_2O_2 yield, electron transfer number, and LSV curves at varied rotating rates, characterization of catalysts after ORR CV cycles, chronoamperometric tests of for ORR; characterization of catalysts after OER CV cycles, chronopotentiometry test for OER, overall LSV curves; photograph of the Zn−air batteries; chronopotentiometry test for HER, characterization of catalysts after HER CV cycles (PDF)

■ AUTHOR INFORMATION

Corresponding Author

Rufan Zhang − *Beijing Key Laboratory of Green Chemical Reaction Engineering and Technology, Department of Chemical Engineering, Tsinghua University, Beijing 100084, China;* orcid.org/0000-0003-1774-0550; Email: zhangrufan@tsinghua.edu.cn

Authors

Chenhui Zhou − *Beijing Key Laboratory of Green Chemical Reaction Engineering and Technology, Department of Chemical Engineering, Tsinghua University, Beijing 100084, China*

Siming Zhao − *Beijing Key Laboratory of Green Chemical Reaction Engineering and Technology, Department of Chemical Engineering, Tsinghua University, Beijing 100084, China*

Haibing Meng − *Beijing Key Laboratory of Green Chemical Reaction Engineering and Technology, Department of Chemical Engineering, Tsinghua University, Beijing 100084, China;* orcid.org/0000-0002-9538-3352

Ying Han − *Beijing Key Laboratory of Green Chemical Reaction Engineering and Technology, Department of Chemical Engineering, Tsinghua University, Beijing 100084, China*

Qinyuan Jiang − *Beijing Key Laboratory of Green Chemical Reaction Engineering and Technology, Department of Chemical Engineering, Tsinghua University, Beijing 100084, China;* orcid.org/0000-0003-4536-6228

Baoshun Wang − *Beijing Key Laboratory of Green Chemical Reaction Engineering and Technology, Department of Chemical Engineering, Tsinghua University, Beijing 100084, China*

Xiaofei Shi − *Beijing Key Laboratory of Green Chemical Reaction Engineering and Technology, Department of Chemical Engineering, Tsinghua University, Beijing 100084, China;* orcid.org/0000-0001-6934-5427

Wenshuo Zhang − *Beijing Key Laboratory of Green Chemical Reaction Engineering and Technology, Department of Chemical Engineering, Tsinghua University, Beijing 100084, China*

Liang Zhang − *Center for Combustion Energy, School of Vehicle and Mobility, Tsinghua University, Beijing 100084, China;* orcid.org/0000-0002-9718-0436

Complete contact information is available at: https://pubs.acs.org/10.1021/acs.nanolett.1c03407

Author Contributions

C.Z. and R.Z. proposed the main idea. R.Z. guided the project. C.Z. designed and conducted the experiments and wrote the paper. L.Z., S.Z., H.M., Y.H., Q.J., B.W., X.S., and W.Z. participated in the data analysis and discussions. The final manuscript was discussed by all authors.

Funding

This study was supported by the National Natural Science Foundation of China (Grants 51872156 and 22075163), National Key Research Program (Grants 2020YFC2201103 and 2020YFA0210702), and China Postdoctoral Science Foundation funded project (Grant 2020M670343).

Notes

The authors declare no competing financial interest.

■ ACKNOWLEDGMENTS

The authors acknowledge the assistance of the Analytical and Testing Center of Tsinghua University for XRD, XPS, BET, SEM, and TEM measurements.

■ REFERENCES

(1) Tian, X.; Zhao, X.; Su, Y.-Q.; Wang, L.; Wang, H.; Dang, D.; Chi, B.; Liu, H.; Hensen, E. J. M.; Lou, X. W.; Xia, B. Y. Engineering bunched Pt-Ni alloy nanocages for efficient oxygen reduction in practical fuel cells. *Science* **2019**, *366*, 850.

(2) Bu, L.; Zhang, N.; Guo, S.; Zhang, X.; Li, J.; Yao, J.; Wu, T.; Lu, G.; Ma, J.-Y.; Su, D.; Huang, X. Biaxially strained PtPb/Pt core/shell nanoplate boosts oxygen reduction catalysis. *Science* **2016**, *354*, 1410.

(3) Dotan, H.; Landman, A.; Sheehan, S. W.; Malviya, K. D.; Shter, G. E.; Grave, D. A.; Arzi, Z.; Yehudai, N.; Halabi, M.; Gal, N.; Hadari, N.; Cohen, C.; Rothschild, A.; Grader, G. S. Decoupled hydrogen and oxygen evolution by a two-step electrochemical-chemical cycle for efficient overall water splitting. *Nat. Energy* **2019**, *4*, 786−795.

(4) Kim, N.-I.; Sa, Y. J.; Yoo, T. S.; Choi, S. R.; Afzal, R. A.; Choi, T.; Seo, Y.-S.; Lee, K.-S.; Hwang, J. Y.; Choi, W. S.; Joo, S. H.; Park, J.-Y. Oxygen-deficient triple perovskites as highly active and durable bifunctional electrocatalysts for oxygen electrode reactions. *Sci. Adv.* **2018**, *4*, No. eaap9360.

(5) Yu, J.; Li, B.-Q.; Zhao, C.-X.; Liu, J.-N.; Zhang, Q. Asymmetric air cathode design for enhanced interfacial electrocatalytic reactions in high-performance zinc-air batteries. *Adv. Mater.* **2020**, *32*, 1908488.

(6) Tiwari, J. N.; Dang, N. K.; Sultan, S.; Thangavel, P.; Jeong, H. Y.; Kim, K. S. Multi-heteroatom-doped carbon from waste-yeast biomass for sustained water splitting. *Nat. Sustain.* **2020**, *3*, 556−563.

(7) Yu, J.; Wang, Y.; Kong, L.; Chen, S.; Zhang, S. Neuron-mimic smart electrode: a two-dimensional multiscale synergistic strategy for densely packed and high-rate lithium storage. *ACS Nano* **2019**, *13*, 9148−9160.

(8) Tang, T.; Jiang, W.-J.; Liu, X.-Z.; Deng, J.; Niu, S.; Wang, B.; Jin, S.-F.; Zhang, Q.; Gu, L.; Hu, J.-S.; Wan, L.-J. Metastable rock salt oxide-mediated synthesis of high-density dual-protected M@NC for long-life rechargeable zinc-air batteries with record power density. *J. Am. Chem. Soc.* **2020**, *142*, 7116−7127.

(9) Yu, F.; Zhou, H.; Huang, Y.; Sun, J.; Qin, F.; Bao, J.; Goddard, W. A.; Chen, S.; Ren, Z. High-performance bifunctional porous non-noble metal phosphide catalyst for overall water splitting. *Nat. Commun.* **2018**, *9*, 2551.

(10) Yang, H. B.; Miao, J.; Hung, S.-F.; Chen, J.; Tao, H. B.; Wang, X.; Zhang, L.; Chen, R.; Gao, J.; Chen, H. M.; Dai, L.; Liu, B. Identification of catalytic sites for oxygen reduction and oxygen evolution in N-doped graphene materials: Development of highly efficient metal-free bifunctional electrocatalyst. *Sci. Adv.* **2016**, *2*, No. e1501122.

(11) Luo, M.; Zhao, Z.; Zhang, Y.; Sun, Y.; Xing, Y.; Lv, F.; Yang, Y.; Zhang, X.; Hwang, S.; Qin, Y.; Ma, J.-Y.; Lin, F.; Su, D.; Lu, G.; Guo,

S. PdMo bimetallene for oxygen reduction catalysis. *Nature* **2019**, *574*, 81−85.
(12) Adabi, H.; Shakouri, A.; Ul Hassan, N.; Varcoe, J. R.; Zulevi, B.; Serov, A.; Regalbuto, J. R.; Mustain, W. E. High-performing commercial Fe-N-C cathode electrocatalyst for anion-exchange membrane fuel cells. *Nat. Energy* **2021**, *6*, 834−843.
(13) Hao, S.; Liu, M.; Pan, J.; Liu, X.; Tan, X.; Xu, N.; He, Y.; Lei, L.; Zhang, X. Dopants fixation of ruthenium for boosting acidic oxygen evolution stability and activity. *Nat. Commun.* **2020**, *11*, 5368.
(14) Chen, R.; Hung, S.-F.; Zhou, D.; Gao, J.; Yang, C.; Tao, H.; Yang, H. B.; Zhang, L.; Zhang, L.; Xiong, Q.; Chen, H. M.; Liu, B. Layered structure causes bulk NiFe layered double hydroxide unstable in alkaline oxygen evolution reaction. *Adv. Mater.* **2019**, *31*, 1903909.
(15) Zhou, K. L.; Wang, Z.; Han, C. B.; Ke, X.; Wang, C.; Jin, Y.; Zhang, Q.; Liu, J.; Wang, H.; Yan, H. Platinum single-atom catalyst coupled with transition metal/metal oxide heterostructure for accelerating alkaline hydrogen evolution reaction. *Nat. Commun.* **2021**, *12*, 3783.
(16) Deng, S.; Luo, M.; Ai, C.; Zhang, Y.; Liu, B.; Huang, L.; Jiang, Z.; Zhang, Q.; Gu, L.; Lin, S.; Wang, X.; Yu, L.; Wen, J.; Wang, J.; Pan, G.; Xia, X.; Tu, J. Synergistic doping and intercalation: realizing deep phase modulation on MoS_2 arrays for high-efficiency hydrogen evolution reaction. *Angew. Chem., Int. Ed.* **2019**, *58*, 16289−16296.
(17) Zhang, Y.; Luo, M.; Yang, Y.; Li, Y.; Guo, S. Advanced multifunctional electrocatalysts for energy conversion. *ACS Energy Lett.* **2019**, *4*, 1672−1680.
(18) Dresp, S.; Luo, F.; Schmack, R.; Kühl, S.; Gliech, M.; Strasser, P. An efficient bifunctional two-component catalyst for oxygen reduction and oxygen evolution in reversible fuel cells, electrolyzers and rechargeable air electrodes. *Energy Environ. Sci.* **2016**, *9*, 2020−2024.
(19) Jin, Y.; Wang, H.; Li, J.; Yue, X.; Han, Y.; Shen, P. K.; Cui, Y. Porous MoO_2 nanosheets as non-noble bifunctional electrocatalysts for overall water splitting. *Adv. Mater.* **2016**, *28*, 3785−3790.
(20) Zhang, Z.; Zhao, X.; Xi, S.; Zhang, L.; Chen, Z.; Zeng, Z.; Huang, M.; Yang, H.; Liu, B.; Pennycook, S. J.; Chen, P. Atomically dispersed cobalt trifunctional electrocatalysts with tailored coordination environment for flexible rechargeable Zn-air battery and self-driven water splitting. *Adv. Energy Mater.* **2020**, *10*, 2002896.
(21) Wang, H.; Lee, H.-W.; Deng, Y.; Lu, Z.; Hsu, P.-C.; Liu, Y.; Lin, D.; Cui, Y. Bifunctional non-noble metal oxide nanoparticle electrocatalysts through lithium-induced conversion for overall water splitting. *Nat. Commun.* **2015**, *6*, 7261.
(22) Wang, S.; Wang, H.; Huang, C.; Ye, P.; Luo, X.; Ning, J.; Zhong, Y.; Hu, Y. Trifunctional electrocatalyst of N-doped graphitic carbon nanosheets encapsulated with CoFe alloy nanocrystals: The key roles of bimetal components and high-content graphitic-N. *Appl. Catal., B* **2021**, *298*, 120512.
(23) Liu, X.; Liu, W.; Ko, M.; Park, M.; Kim, M. G.; Oh, P.; Chae, S.; Park, S.; Casimir, A.; Wu, G.; Cho, J. Metal (Ni, Co)-metal oxides/graphene nanocomposites as multifunctional electrocatalysts. *Adv. Funct. Mater.* **2015**, *25*, 5799−5808.
(24) Shi, Q.; Liu, Q.; Ma, Y.; Fang, Z.; Liang, Z.; Shao, G.; Tang, B.; Yang, W.; Qin, L.; Fang, X. High-performance trifunctional electrocatalysts based on FeCo/Co_2P hybrid nanoparticles for zinc-air battery and self-powered overall water splitting. *Adv. Energy Mater.* **2020**, *10*, 1903854.
(25) Liu, H.; Guan, J.; Yang, S.; Yu, Y.; Shao, R.; Zhang, Z.; Dou, M.; Wang, F.; Xu, Q. Metal-organic-framework-derived Co_2P nanoparticle/multi-doped porous carbon as a trifunctional electrocatalyst. *Adv. Mater.* **2020**, *32*, 2003649.
(26) Kong, F.; Fan, X.; Kong, A.; Zhou, Z.; Zhang, X.; Shan, Y. Covalent phenanthroline framework derived FeS@Fe_3C composite nanoparticles embedding in N-S-Co doped carbons as highly efficient trifunctional electrocatalysts. *Adv. Funct. Mater.* **2018**, *28*, 1803973.
(27) Mahmood, A.; Tabassum, H.; Zhao, R.; Guo, W.; Aftab, W.; Liang, Z.; Sun, Z.; Zou, R. Fe_2N/S/N codecorated hierarchical porous carbon nanosheets for trifunctional electrocatalysis. *Small* **2018**, *14*, 1803500.
(28) Li, H.; Li, Q.; Wen, P.; Williams, T. B.; Adhikari, S.; Dun, C.; Lu, C.; Itanze, D.; Jiang, L.; Carroll, D. L.; Donati, G. L.; Lundin, P. M.; Qiu, Y.; Geyer, S. M. Colloidal cobalt phosphide nanocrystals as trifunctional electrocatalysts for overall water splitting powered by a zinc-air battery. *Adv. Mater.* **2018**, *30*, 1705796.
(29) Sun, Y.; Huang, B.; Li, Y.; Xing, Y.; Luo, M.; Li, N.; Xia, Z.; Qin, Y.; Su, D.; Wang, L.; Guo, S. Trifunctional fishbone-like PtCo/Ir enables high-performance zinc-air batteries to drive the water-splitting catalysis. *Chem. Mater.* **2019**, *31*, 8136−8144.
(30) Zhang, W.; Zhao, J.; Zhang, J.; Chen, X.; Zhang, X.; Yang, F. Electronic asymmetric distribution of RhCu bimetallic nanocrystals for enhancing trifunctional electrocatalysis. *ACS Appl. Mater. Interfaces* **2020**, *12*, 10299−10306.
(31) Qin, Q.; Jang, H.; Chen, L.; Nam, G.; Liu, X.; Cho, J. Low loading of Rh_xP and RuP on N, P codoped carbon as two trifunctional electrocatalysts for the oxygen and hydrogen electrode reactions. *Adv. Energy Mater.* **2018**, *8*, 1801478.
(32) Bai, L.; Duan, Z.; Wen, X.; Si, R.; Zhang, Q.; Guan, J. Highly dispersed ruthenium-based multifunctional electrocatalyst. *ACS Catal.* **2019**, *9*, 9897−9904.
(33) Zhu, B.; Qu, C.; Gao, S.; Liang, Z.; Zhang, H.; Zou, R. Ultralow loading ruthenium nanoparticles on nitrogen-doped graphene aerogel for trifunctional electrocatalysis. *ChemCatChem* **2018**, *10*, 1113−1121.
(34) Tao, H. B.; Fang, L.; Chen, J.; Yang, H. B.; Gao, J.; Miao, J.; Chen, S.; Liu, B. Identification of surface reactivity descriptor for transition metal oxides in oxygen evolution reaction. *J. Am. Chem. Soc.* **2016**, *138*, 9978−9985.
(35) Ji, D.; Fan, L.; Tao, L.; Sun, Y.; Li, M.; Yang, G.; Tran, T. Q.; Ramakrishna, S.; Guo, S. The kirkendall effect for engineering oxygen vacancy of hollow Co_3O_4 nanoparticles toward high-performance portable zinc-air batteries. *Angew. Chem., Int. Ed.* **2019**, *58*, 13840−13844.
(36) Lu, Q.; Guo, Y.; Mao, P.; Liao, K.; Zou, X.; Dai, J.; Tan, P.; Ran, R.; Zhou, W.; Ni, M.; Shao, Z. Rich atomic interfaces between sub-1 nm RuO_x clusters and porous Co_3O_4 nanosheets boost oxygen electrocatalysis bifunctionality for advanced Zn-air batteries. *Energy Storage Mater.* **2020**, *32*, 20−29.
(37) Li, Z.; Niu, W.; Yang, Z.; Zaman, N.; Samarakoon, W.; Wang, M.; Kara, A.; Lucero, M.; Vyas, M. V.; Cao, H.; Zhou, H.; Sterbinsky, G. E.; Feng, Z.; Du, Y.; Yang, Y. Stabilizing atomic Pt with trapped interstitial F in alloyed PtCo nanosheets for high-performance zinc-air batteries. *Energy Environ. Sci.* **2020**, *13*, 884−895.
(38) Xia, Z.; Fang, J.; Zhang, X.; Fan, L.; Barlow, A. J.; Lin, T.; Wang, S.; Wallace, G. G.; Sun, G.; Wang, X. Pt nanoparticles embedded metal-organic framework nanosheets: A synergistic strategy towards bifunctional oxygen electrocatalysis. *Appl. Catal., B* **2019**, *245*, 389−398.
(39) Sun, Y.; Zhang, X.; Luo, M.; Chen, X.; Wang, L.; Li, Y.; Li, M.; Qin, Y.; Li, C.; Xu, N.; Lu, G.; Gao, P.; Guo, S. Ultrathin PtPd-based nanorings with abundant step atoms enhance oxygen catalysis. *Adv. Mater.* **2018**, *30*, 1802136.
(40) Han, J.; Meng, X.; Lu, L.; Wang, Z. L.; Sun, C. Triboelectric nanogenerators powered electrodepositing tri-functional electrocatalysts for water splitting and rechargeable zinc-air battery: A case of Pt nanoclusters on NiFe-LDH nanosheets. *Nano Energy* **2020**, *72*, 104669.
(41) Zhu, J.; Xie, M.; Chen, Z.; Lyu, Z.; Chi, M.; Jin, W.; Xia, Y. Pt-Ir-Pd trimetallic nanocages as a dual catalyst for efficient oxygen reduction and evolution reactions in acidic media. *Adv. Energy Mater.* **2020**, *10*, 1904114.
(42) Zhuang, L.; Jia, Y.; Liu, H.; Wang, X.; Hocking, R. K.; Liu, H.; Chen, J.; Ge, L.; Zhang, L.; Li, M.; Dong, C.-L.; Huang, Y.-C.; Shen, S.; Yang, D.; Zhu, Z.; Yao, X. Defect-induced Pt-Co-Se coordinated sites with highly asymmetrical electronic distribution for boosting oxygen-involving electrocatalysis. *Adv. Mater.* **2019**, *31*, 1805581.
(43) Bian, Y.; Wang, H.; Gao, Z.; Hu, J.; Liu, D.; Dai, L. A facile approach to high-performance trifunctional electrocatalysts by

https://doi.org/10.1021/acs.nanolett.1c03407
Nano Lett. 2021, 21, 9633−9641

substrate-enhanced electroless deposition of Pt/NiO/Ni on carbon nanotubes. *Nanoscale* **2020**, *12*, 14615−14625.
(44) Hu, S.; Goenaga, G.; Melton, C.; Zawodzinski, T. A.; Mukherjee, D. $PtCo/CoO_x$ nanocomposites: Bifunctional electrocatalysts for oxygen reduction and evolution reactions synthesized via tandem laser ablation synthesis in solution-galvanic replacement reactions. *Appl. Catal., B* **2016**, *182*, 286−296.
(45) Kwak, I.; Kwon, I. S.; Kim, J.; Park, K.; Ahn, J.-P.; Yoo, S. J.; Kim, J.-G.; Park, J. IrO_2-ZnO hybrid nanoparticles as highly efficient trifunctional electrocatalysts. *J. Phys. Chem. C* **2017**, *121*, 14899−14906.
(46) Park, H.-S.; Seo, E.; Yang, J.; Lee, Y.; Kim, B.-S.; Song, H.-K. Bifunctional hydrous RuO_2 nanocluster electrocatalyst embedded in carbon matrix for efficient and durable operation of rechargeable zinc-air batteries. *Sci. Rep.* **2017**, *7*, 7150.
(47) Park, J.; Risch, M.; Nam, G.; Park, M.; Shin, T. J.; Park, S.; Kim, M. G.; Shao-Horn, Y.; Cho, J. Single crystalline pyrochlore nanoparticles with metallic conduction as efficient bi-functional oxygen electrocatalysts for Zn-air batteries. *Energy Environ. Sci.* **2017**, *10*, 129−136.
(48) Yoon, K. R.; Lee, G. Y.; Jung, J.-W.; Kim, N.-H.; Kim, S. O.; Kim, I.-D. One-dimensional RuO_2/Mn_2O_3 hollow architectures as efficient bifunctional catalysts for lithium-oxygen batteries. *Nano Lett.* **2016**, *16*, 2076−2083.
(49) Tao, H. B.; Zhang, J.; Chen, J.; Zhang, L.; Xu, Y.; Chen, J. G.; Liu, B. Revealing energetics of surface oxygen redox from kinetic fingerprint in oxygen electrocatalysis. *J. Am. Chem. Soc.* **2019**, *141*, 13803−13811.
(50) Liang, Y.; Li, Y.; Wang, H.; Zhou, J.; Wang, J.; Regier, T.; Dai, H. Co_3O_4 nanocrystals on graphene as a synergistic catalyst for oxygen reduction reaction. *Nat. Mater.* **2011**, *10*, 780−786.
(51) Wang, Z.; Xu, W.; Chen, X.; Peng, Y.; Song, Y.; Lv, C.; Liu, H.; Sun, J.; Yuan, D.; Li, X.; Guo, X.; Yang, D.; Zhang, L. Defect-rich nitrogen doped Co_3O_4/C porous nanocubes enable high-efficiency bifunctional oxygen electrocatalysis. *Adv. Funct. Mater.* **2019**, *29*, 1902875.
(52) Liu, J.; Zheng, Y.; Jiao, Y.; Wang, Z.; Lu, Z.; Vasileff, A.; Qiao, S.-Z. NiO as a bifunctional promoter for RuO_2 toward superior overall water splitting. *Small* **2018**, *14*, 1704073.
(53) Xue, T.; Wang, X.; Lee, J.-M. Dual-template synthesis of $Co(OH)_2$ with mesoporous nanowire structure and its application in supercapacitor. *J. Power Sources* **2012**, *201*, 382−386.
(54) Wang, C.; Qi, L. Heterostructured inter-doped ruthenium-cobalt oxide hollow nanosheet arrays for highly efficient overall water splitting. *Angew. Chem., Int. Ed.* **2020**, *59*, 17219−17224.

https://doi.org/10.1021/acs.nanolett.1c03407
Nano Lett. 2021, 21, 9633−9641